CSC8316 Assessment Two

Raman Chahal, 160067554

Word count: 2,651

1 Introduction

B. Subtilis is one of the most well characterised bacterial organisms, being a model system for cell differentiation and development. It is a Gram-positive bacterium which can tolerate harsh environmental conditions, as endospore formation under nutritional stress allows the organisms to persevere in factors such as acid, salt and heat, until the environment becomes more favourable (Sonenshein AL, *et al*., 2002).

The robustness of *B. Subtilis* is one of the many reasons why it is used by academia and as an industrial workhorse, as well as the fact that it is 'Generally Regarded as Safe' (GRAS) by the US Food and Drug Administration (Vincent S, *et al*., 2016), and so is used as a safer substitute for pathogenic strains of bacillus. Furthermore, *B. Subtilis* has been shown to grow fast, allowing for short production cycles (Kabisch J, *et al*., 2013).

B. Subtilis produces a variety of useful compounds that have a diverse number of applications in the pharmaceutical, food (fortification) and biofuel industry. For instance, riboflavin (Vitamin B2) is a water insoluble vitamin essential for humans and animals and is used for the applications mentioned above. (S. Shi, *et al*., 2009)

Riboflavin is a precursor to the coenzymes FAD (flavin adenine dinucleotide) and FMN (flavin mononucleotide), which are essential for protein, fat and carbohydrate metabolism, as well as glutathione reductase mediated detoxification – by destroying free radicals (in the liver) (NCBI, PubChem Database, 2019). Riboflavin has also been shown to assist tryptophan to niacin conversion, activating vitamin B6 (Lykstad J, *et al*., 2019). In humans, riboflavin is important for maintaining healthy skin, nails and hair.

Riboflavin deficiency can arise from many developmental abnormalities such as retardation of growth, cleft lip and palate, and cardiac related diseases. Other people at risk of riboflavin deficiency include patients suffering from Brown-Vialetto-Van Laere syndrome (BVVL), pregnant and lactating women, and vegan people. Riboflavin deficiency can lead to anaemia, by alteration of iron absorption, migraines, cataracts, glaucoma, keratoconus, and thyroid dysfunction. (Balasubramaniam S, *et al*., 2019; Finsterer J, *et al*., 2018; Peechakara BV, *et al*., 2019)

The large-scale production of riboflavin for commercial applications typically relies on microbial one-step fermentation of favinogenic microorganisms with A*shbya gossypii* and *Bacillus subtilis* as the main vitamin producers (Stahmann KP, *et al*., 2000). The process of fermentation involves growing *B. Subtilis* cultures in a glucose-limited fed-batch fermentation, followed by pasteurisation of the fermentation broth. Riboflavin crystals accumulate in the fermentation medium and are separated from the bacillus cells by differential centrifugation, followed by washing with hot mineral acid (Figure 1) (Kupfer E, *et al*., 1995)

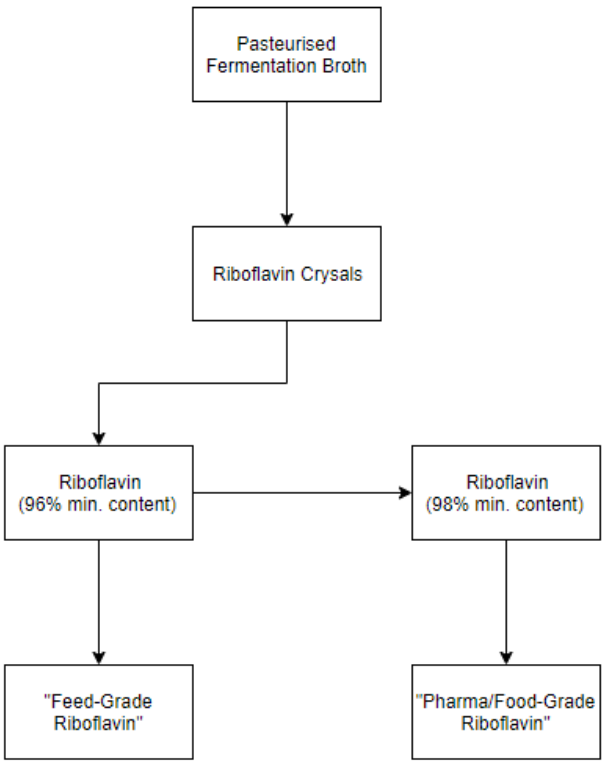

Figure 1. Production of riboflavin from fermentation broth. The method is summarised above where the % content values refer to the minimum guaranteed content of the product according to Bretzel et al (Bretzel W, *et al*., 1999)

In *Bacillus Subtilis* the enzyme Riboflavin Synthase catalyses the formation of riboflavin (and 5-amino-2,6-dihydroxy-4-pyrimidine) from two 6,7-dimethyl-8-(D-ribityl)lumazine molecules. An overview of riboflavin production in *B. Subtilis* is shown in figure 2.

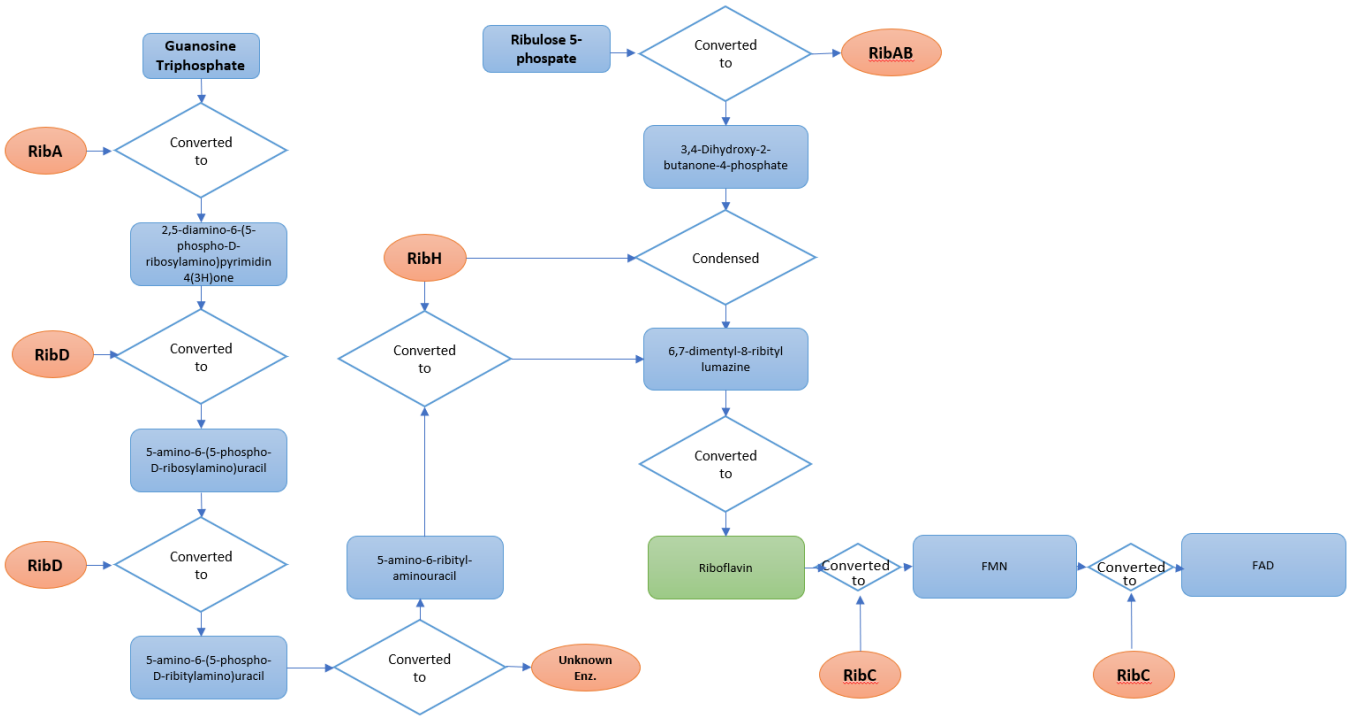

Figure 2. Overview schematic of riboflavin production in *B. Subtilis*. Metabolites are shown in blue and proteins shown in orange.

It has been shown that there are two types of riboflavin synthases, characterised by the structures of its subunits: heavy synthase ($\alpha_3\beta_{60}$) and light synthase (α_3). Interestingly, the β subunit of the heavy enzyme has been described in detail. Both the primary structure and 3D structure of the 16kDa protein has been determined by x-ray crystallography (Ludwig HC, *et al*., 1987; Ladenstein R, *et al*., 1988). The same cannot be said for the α-subunit, which functions as the core of the heavy enzyme and as light riboflavin synthase. Crystallography studies have not shown any relevant information for the alpha subunit (Ladenstein R, *et al*., 1988).

Genome-scale computational models of metabolic networks are increasing in popularity as they are efficient tools in metabolic phenotype studies. A 2013 study led by Hao T developed a genome-scale metabolic network of *B. subtilis*, which was used for *in silico* metabolic engineering of the bacteria in efforts for increasing the production of riboflavin (Hao T *et al*., 2013). Whole genome sequencing of *B. Subtilis* has assisted genetic engineering design for industrial purposes (F. Kunst, *et al*., 1997), however further improvement of bacterial strains, by modifying genes to alleviate likely genetic bottlenecks (Z. Zhang, *et al*., 2009), is still desired. It is becoming increasingly difficult to identify these bottlenecks as more is known about the complexity of *B. Subtilis*. The fast and accurate predicative nature of genome-wide metabolic network models of *B. Subtilis* on gene knockout and environmental fluctuations has been demonstrated as a crucial tool in metabolic studies; by being able to interpret experimental data and provide supportive predictions on the metabolic phenotype (I. Thiele, *et al*., 2010; M. Durot, *et al*., 2009; H. U. Kim, *et al*., 2012). These predications open more options for designing *in vivo* experiments to enhance strain efficacy.

Recombinant strains of B. Subtilis have been developed in collaboration between Hoffmann-La Roche Ltd and OmniGene Bioproducts Inc, introducing mutations in the RIBC gene which affect purine pathway regulation, and introduce resistance against roseoflavin (an analogue of riboflavin). RibC is the kinase responsible for the conversion of riboflavin to the active co-factors FAD and FMN. The introduced mutation reduces the activity of RibC, resulting in a reduction in the repressive effects of FMN on riboflavin production, thus increasing riboflavin yield (Coquard D, *et al*., 1997; Mack M, *et al*., 1998).

Modelling the enzyme-catalysed reactions for riboflavin biogenesis starts with reversible binding of a substrate (S) with an enzyme (E). An enzyme-substrate complex is formed, where S is converted to product (P) once the enzyme has been released:

$$S + E \underset{k1r}{\overset{k1}{\rightleftarrows}} ES \xrightarrow{k2} E + P$$

$$v1 = k1[S][E], \quad v1r = k1r[ES], \quad v2 = k2[ES]$$

The reactions for the series of single-substrate enzyme reaction mechanism (Figure 13) can be portrayed using differential rate equations (Chen L, *et al*., 2009):

```
dS/dt  = k1r*ES - k1*S*E
dE/dt  = k1r*ES + k2*ES - k1*S*E
dES/dt = k1*S*E - k1r*ES - k2*ES
dP/dt  = k2*ES
```

Reaction: S + E -> ES

Reaction rate: k1*S*E (binding)

Reaction: ES -> S + E

Reaction rate: k1r*ES (unbinding)

Reaction: ES -> E + P

Reaction rate: k2*ES (transformation)

Ordinary differential equation (ODE) models are used to describe quantitative species concentration, to show detailed dynamic behaviours of components within the model This is achieved by using continuous state variables and literature-based parameters across a continuous timescale (de Jong H, *et al*., 2002). The predicted model and experimental data can therefore be compared to increase the model's accuracy.

Rule-based modelling is used to avoid enumeration of chemical species in a system when modelling a biomolecular interaction network (Le Novère N, *et al*., 2013). Once the rule-based model has been established, switching between stochastic and deterministic simulation methods is made easier. Equation-based models are centered around assumptions on chemical species population, so the size of the model represents the number of chemical species within a system. Comparatively, rule-based models are centered around modularity of interactions, so the model size relates to the number of interactions of interest.

While ODE (and RuleBased) models are useful, they inherently assume the observed dynamics are solely driven by internal mechanistic factors, ignoring how the biological system, in practice, will be exposed to influences that are not fully realised and cannot be clearly modelled (Vannitsem S, *et al*., 2014). Therefore, extending these deterministic models to incorporate more convoluted fluctuations in the dynamics would yield a more representative model. Models that accomplish this are known as stochastic models, as they introduce stochastic "noise".

Flux Balance Analysis (FBA) mathematically analyses the flow of metabolites in a biochemical network. FBA involves adding additional constrains to a stoichiometric network (Ledesma-Amaro, *et al*., 2015), allowing accurate predication of the production rate of a metabolite of interest, in this case riboflavin. Applying constraints allows maximisation of the biomass reactions, thus the fluxes which do this were observed.

2 Methods

2.1 Entity – Relationship Diagram

An entity relationship diagram (Chen notation) of riboflavin production in B. Subtilis was completed in 'draw.io' based on the KEGG pathway of riboflavin metabolism in Bacillus subtilis subsp. subtilis 16. The relationships (diamond box) between the entity types (rectangular box) are shown outlying the pathway in a high form of abstraction. (Figure 3)

2.2 Protein-Interaction Map

Using information gathered in STRING a protein-interaction map of key proteins involved in the production of riboflavin in Bacillus Subtilis was created in Cytoscape 3.7.1. Two metabolites are included in the drawing (5-amino-6-(D- ribitylamino)uracil and 3,4-dihydroxy-2-butanone 4-phosphate), with their interaction with ribH highlighted (Figure 4). The black line connecting each protein (edge) represents an interaction, where the nature of these interactions is noted in the edge table (Figure 6). The node table contains information about the protein for each respective node, including enzyme classification number and protein function (Figure 5). The stepwise process of creating the protein-interaction map in Cytoscape is demonstrated in Figure 7.

Using STRING, RibE network was examined to identify the NusB protein, which is shown to be involved in controlling the length of ribE RNA transcripts by transcription antitermination (Figure 8A). Searching for RibE (B. Subtilis) in STRING and pressing 'more' allowed NusB to be visible in the protein-interaction network. Another regulatory protein, RibR, was shown to interact with RibE indirectly with RibAB. This protein is suggested to be involved in regulating rib genes as shown in Figure 8D,

which may play a role in ribE RNA transcript length control.

2.3 Ondex

Further exploration of interacting proteins in the riboflavin biosynthesis network (*B.* Subtilis) was carried out in Ondex – Knet Builder 2.1 using BacillOndex datasets. Searching for RibA (enzyme) in the dataset with neighbourhood depth set to 2, making sure the graph layout was in Gem format, displayed that RibAB has magnesium, zinc and manganese binding sites (Figure 9A, B).

In the search results for 'ribA', selecting the operon ypuE-ribDEAHT and filtering the graph (dataset with neighbourhood depth set to 2) visualised ribAB to be part of the operon, as shown in Figure 9E. Figure 9 shows an overview of the process to obtain this data in Ondex.

2.4 Dynamic Modelling

To follow the changes of riboflavin production *in B. Subtilis* over time a dynamic model of riboflavin synthesis in *B. Subtilis* was produced using Antimony (Spyder for Tellurium 3.6), consisting of an ODE system following the law of mass action (Aronson JK, *et al*., 2016). The single equations in Figure X represent the mass balances for metabolites involved in biosynthesis.

The generated SBML (Systems Biology Mark-up Language) was simulated in CopasiUI 4.25 to display the concentration of riboflavin over time. CopasiUI allowed the properties of the simulation to be changed, so the solution of the ODEs of the model were computed over 100 seconds with increments of 0.1 seconds.

In order to analyse the dynamic behaviour of riboflavin synthesis, three separate ODE models were made in Tellurium. The first model used reactions 1-3 (Figure 13) and the concentration of riboflavin at highest point (Vmax) recorded. The second model includes all reactions in the first model along with reactions 4 and 5 (Figure 13); the third model uses reactions 1-7 and riboflavin concentration at Vmax was reported.

2.5 RuleBased Modelling

A rule-based model of riboflavin production in *B. Subtilis* was created using BioNetGen language (BNGL) in RuleBender. Once the BNGL-encoded model was specified, it was translated into SBML format for use in CopasiUI to generate graphs representing Riboflavin concentration changes over time using the same three separate reactions models used in the Tellurium Model.

2.6 Stochastic Modelling

The concentrations and rate parameters of the Michaelis-Menten enzymic reactions were converted for SSA in BioNetGen. The deterministic rate constants k1, k1r, and k2 were converted into the stochastic rate constants c1, c1r and c2 using the method outlined in Table 1 before simulating the SSA.

Enzyme Reaction Type	Reaction Form	Propensity	Deterministic Rate Constants (k)	Rate of Consumption of Reactants	Stochastic rate constants (c)
$E + S \rightarrow ES$	X + Y → Z	cxy	k1	$\frac{k}{nAV}$	c1 $= \frac{k1}{nAV}$
$ES \rightarrow ES + S$	X → Y	cx	k1r	$knA[X]V$	c1r = k1r
$ES \rightarrow E + P$	X → Y	cx	k2	$knA[X]V$	c2 = k2

Table 1. Conversion of deterministic rate constants to stochastic rate constants based on the type of enzymatic reaction is displayed. nA is Avogadro's Constant ($6.02214086 \times 10^{23}$ mol^{-1}), and V = 10^{-15}

2.7 Flux Balance Analysis

Flux balance analysis was performed in OptFlux using the Michaelis-Menten enzymic reactions 1-7 (figure 13) SBML model. Two synthesis reactions were created for R5P and GTP, and two biomass reactions created for Riboflavin and FAD (Figure 19). Upper and lower bounds were set for the fluxes (by creating environmental conditions) as described in figure 18. The steady state fluxes were computed by simulating wild type and the results shown in figure 18.

3 Results *(For assignment 2)*

3.1 Dynamic Modelling

For reactions 1-3, the Vmax had not been achieved after 100 seconds (no observed plateau) thus, the concentration of riboflavin at this time was recorded (~ 1.39E-06 mol/l at 100 seconds) (Figure 10).

For reactions 1-5, the concentration of riboflavin at Vmax was ~4.00E-07 mol/l (Figure 11).

The riboflavin concentration at Vmax for reactions 1-7 was observed to be ~3.90E-07 mol/l (Figure 12).

3.2 RuleBased Modelling

The results using RuleBased modelling were shown to be the exact same as the results generated by dynamic modelling in Tellurium. For reactions 1-3, [Riboflavin] at 100 seconds was ~ 1.39E-06 mol/l. For reactions 1-5 and 1-7, the [Riboflavin] at Vmax was reported at ~4.00E-07 mol/l and ~3.90E-07 mol/l respectively (Figure 10-12).

3.3 Stochastic Modelling

After simulation of SSA for reactions 1-3, 1-5 and 1-7 (Figures 14-16) the Vmax of riboflavin was recorded: Reactions 1-3: are shown to be ~ 8.25E02 mol/l at 100 seconds; Reactions 1-5: ~2.50E02 mol/l; Reactions 1-7: ~2.30E02 mol/l.

3.4 Flux Balance Analysis

Net conversions of consumption of R5P shown to be 125 and the net conversion of production of FAD was shown to be 50; and for Riboflavin: 75 (figure 18).

4 Discussion

For the kinetic models (dynamic and rule-based) the concentration of riboflavin was highest using reactions 1-3: ~ 1.39E-06 mol/l compared to ~3.90E-07 mol/l for reactions 1-7 (Figure 10, 12), as there aren't any reactions involved in consuming riboflavin. The same pattern is observed in the stochastic models (Figures 14-16) but the concentrations are different, as the are based on the number of molecules not moles.

After riboflavin is produced, RibC catalyses the conversion of riboflavin to FMN. Therefore, future work including introduction of RibC inhibitors in the kinetic model, to prevent the reaction continuing to produce FMN and FAD (by consuming riboflavin), may increase riboflavin yield from *B. Subtilis*. As Vmax had not been achieved for the model involving reactions 1-3, increasing the duration of the time course until Vmax is reached would return more representative results.

Rib A is involved in both starting points of the riboflavin biogenesis network (Figure 2.), involving conversion of R5P to D2B4P, and GTP to D6P4. The GTP reaction is introduced as reaction 6 for each model, thus when modelling reactions 1-7, the observed global decrease in [riboflavin] was ~0.10E-07 mol/l for dynamic, rule-based and stochastic modelling, when compared to reactions 1-5 (Figure X). This may be attributed to competition for RibA binding sites between GTP and R5P. Therefore, the results suggest RibA is rate limiting in the pathway. To further assess this, increasing the concentration of RibA in the kinetic model and observing the changes in riboflavin concentration would provide further insight whether this hypothesis is true.

In a 2014 study by Birkenmeier *et al* (Birkenmeier, *et al*., 2014), an ODE-based model for riboflavin biosynthesis was created using literature-derived data for production strains. The group's aim was to determine the limiting order for the enzymes involved in the pathway. They confirmed RibA as the most rate-limiting, with the reductase activity of RibG and RibH as the next most limiting step. This supports the data described here.

Flux balance analysis was performed with constraints applied to FAD production, and synthesis of R5P and GTP, allowing maximisation of riboflavin. From figure 18, the rate of production for FAD was 50, and for riboflavin was 75. The higher rate for riboflavin production (in contrast to FAD production) when these constraints are applied would be useful to increase riboflavin yield. Future work would consist of optimization of the constraints so the ratio of riboflavin to FAD production would be further increased. An important limitation of FBA involves the arbitrary selection of a single metabolic state at every time interval from the solution space provided by FBA. This is potentially problematic as the arbitrary choice results in exploration of only a few dynamic flux profiles. Nevertheless, FBA provides a qualitative glimpse of the enzymic events and their effect on metabolism (Covert MW, *et al*., 2002).

In conclusion, this study helps understand how riboflavin is synthesised in the biochemical network, promoting further experimentations. Additional research is required to improve these models for implications in industry. Specifically applying the exact experimentally-derived enzymatic rate laws with respect to substrates and products, along with complete quantification of involved enzymes would improve analysis.

5 Figures

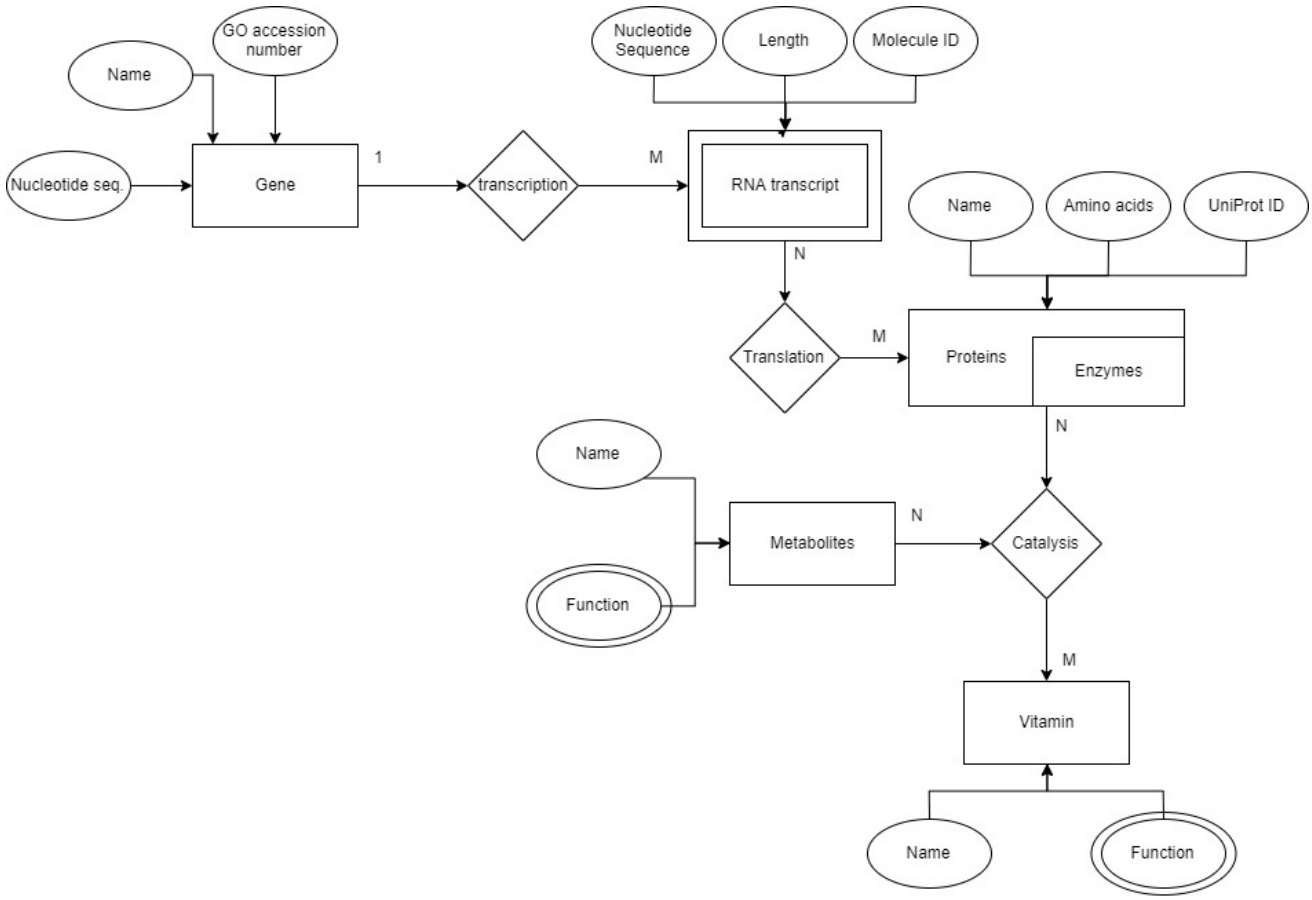

Figure 3. Entity relationship diagram of riboflavin biosynthesis in *Bacillus Subtilis*. Entity-types are represented by the rectangular box, attributes are noted in circles, where a double circle represents a multi-value attribute, and relationships between entity-types are noted by the diamond box.

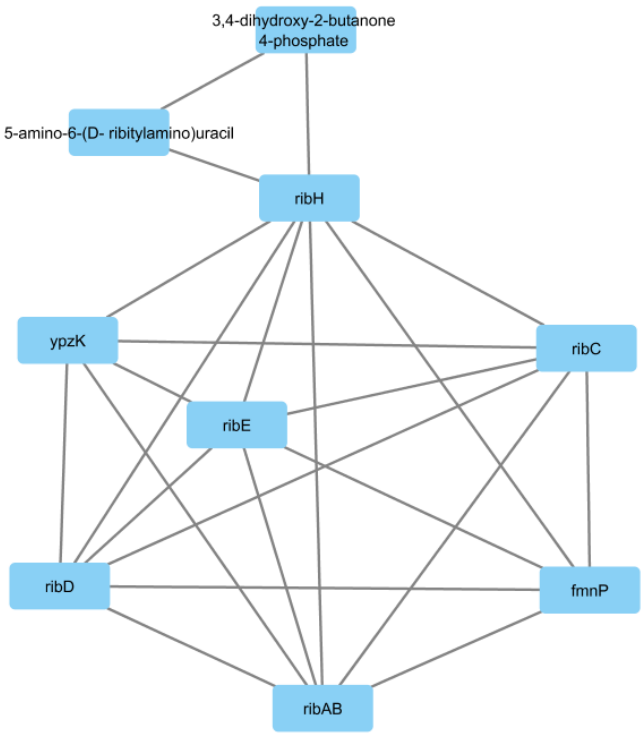

Figure 4. Cytoscape (3.7.1) drawn protein-interaction map of the proteins RibC, FmnP, RibAB, RibD, RibE, RibT (ypzK) and RibH, involved in riboflavin biosynthesis in *Bacillus Subtilis*. Two metabolites (5-amino-6-(D- ribitylamino)uracil and 3,4-dihydroxy-2-butanone 4-phosphate) that interact with RibH are also shown. The lines between the nodes represent an interaction.

	name	Organism	Name of Metabolite	Name of protein	Gene encoding protein
1	ribH	Bacillus subtilis	-	6,7-dimethyl-8-ribityllumazine synthase	ribH
2	ribC	Bacillus subtilis	-	Riboflavin biosynthesis protein RibC	ribC
3	ribE	Bacillus subtilis	-	Riboflavin synthase	ribE
4	ribAB	Bacillus subtilis	-	Riboflavin biosynthesis protein RibBA	ribAB
5	ribD	Bacillus subtilis	-	Riboflavin biosynthesis protein RibD	ribD
6	ypzK	Bacillus subtilis	-	Protein RibT	ypzK
7	fmnP	Bacillus subtilis	-	Riboflavin transporter FmnP	fmnP
8	5-amino-6-(D- ribitylamino)uracil			-	
9	3,4-dihydroxy-2-butanone 4-phosphate			-	

	Enzyme Classification Number	Function of Protein
1	BSU23250	Catalyzes the formation of 6,7-dimethyl-8- ribityllumazine by condensation of 5-amino-6-(D- ribitylamino)uracil with 3,4-dihydroxy-2-butanone 4-phosphate.
2	BSU16670	RibC is a bifunctional riboflavin kinase and FMN adenylyltransferase, catalyzing the final steps in the biosynthesis of FAD
3	BSU23270	Catalyzes the dismutation of two molecules of 6,7- dimethyl-8-ribityllumazine, resulting in the formation of riboflavin and 5-amino-6-(D-ribitylamino)uracil
4	BSU23260	Catalyzes the conversion of D-ribulose 5-phosphate to formate and 3,4-dihydroxy-2-butanone 4-phosphate
5	BSU23280	Converts 2,5-diamino-6-(ribosylamino)-4(3h)-pyrimidinone 5′-phosphate into 5-amino-6-(ribosylamino)-2,4(1h,3h)- pyrimidinedione 5′-phosphate
6	BSU23240	Involved in riboflavin biosynthesis
7	BSU23050	Mediates uptake of riboflavin and roseoflavin, a toxic riboflavin analog; may also transport FMN.
8		Catalyzes the formation of 6,7-dimethyl-8- ribityllumazine by condensation of 5-amino-6-(D- ribitylamino)uracil with 3,4-dihydroxy-2-butanone 4-phosphate.
9		

Figure 5. Node table of the protein-interaction map (Figure 4.) showing the function, gene encoding protein and enzyme classification number of each respective protein. The figure has been split in two, where the number (1-9) refers to each member.

name	interaction
ribH (interacts with) ribC	interacts with
ribH (interacts with) ribE	interacts with
ribH (interacts with) ribAB	interacts with
ribH (interacts with) ribD	interacts with
ribH (interacts with) ypzK	interacts with
ribC (interacts with) ypzK	interacts with
ribC (interacts with) ribD	interacts with
ribC (interacts with) ribAB	interacts with
ribC (interacts with) ribE	interacts with
ribE (interacts with) ypzK	interacts with
ribE (interacts with) ribD	interacts with
ribE (interacts with) ribAB	interacts with
ribAB (interacts with) ypzK	interacts with
ribAB (interacts with) ribD	interacts with
ribD (interacts with) ypzK	interacts with
fmnP (interacts with) ribH	interacts with
fmnP (interacts with) ribC	interacts with
fmnP (interacts with) ribE	interacts with
fmnP (interacts with) ribAB	interacts with
fmnP (interacts with) ribD	interacts with
5-amino-6-(D- ribitylamino)uracil (interacts with) 3,4-dihydroxy-2-butanone 4-phosphate	Interacts with
5-amino-6-(D- ribitylamino)uracil (interacts with) ribH	Is condensed to 6,7-dimethyl-8- ribityllumazine with 3,4-dihydroxy-2-butanone 4-phosphate by RibH
3,4-dihydroxy-2-butanone 4-phosphate (interacts with) ribH	Is condensed to 6,7-dimethyl-8- ribityllumazine with 5-amino-6-(D- ribitylamino)uracil by RibH

Figure 6. Edge table of the protein-interaction map (Figure 4.) highlighting the interactions between each respective protein

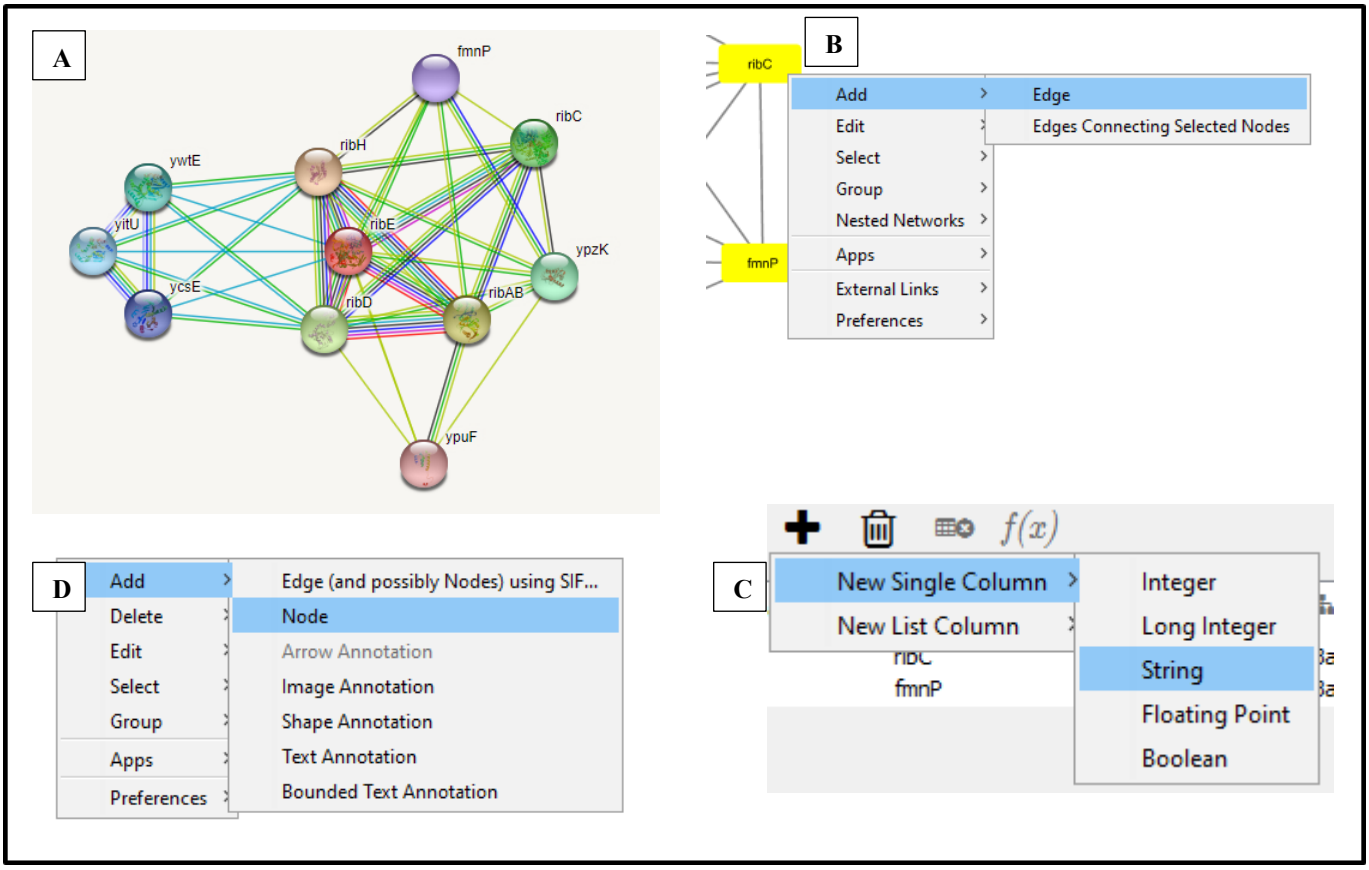

Figure 7. Stepwise process in protein-interaction network building in Cytoscape 3.7.1. **(A)** Protein-interaction map (with RibE (B. Subtilis) as query protein) in STRING provided a template for the one to be drawn in Cytoscape 3.7.1. **(B)** Nodes were created in Cytoscape by right-clicking -> Add -> Node. The nodes were renamed to represent each protein. **(C)** Edges were added between the created nodes by right-clicking -> Add -> Edge Connecting Selected Nodes, after selecting the desired nodes. **(D)** Attributes were added to each of the protein nodes and edges in the node table and edge table by adding New String Single Columns. "Enzyme Classification Numbers" and "Genes encoding protein" were sourced using STRING.

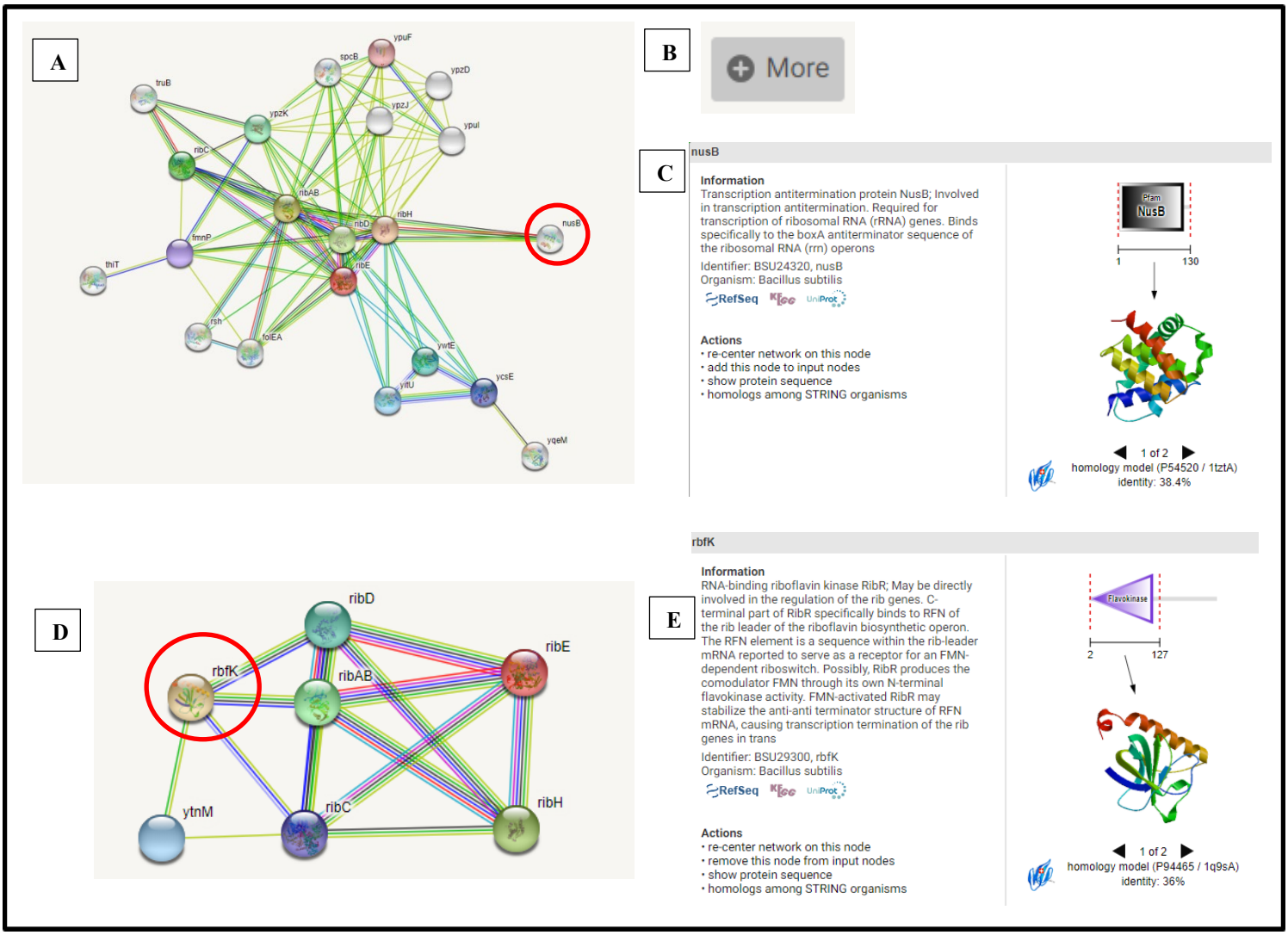

Figure 8. RibE network examined in STRING **(A)** after pressing "more" **(B)** to show more interacting partners. Protein NusB, as highlighted by the red circle, is shown to interact with the RibE network and is described as a transcription antitermination protein **(C)**, suggesting its use in *ribE* RNA transcript length control. Further expansion of the RibE network in STRING **(D)** identified RibR protein, which may also be involved in controlling the length of *ribE* RNA transcripts. RibR, as highlighted by the red circle, is shown to be involved in *rib* gene regulation **(E)**.

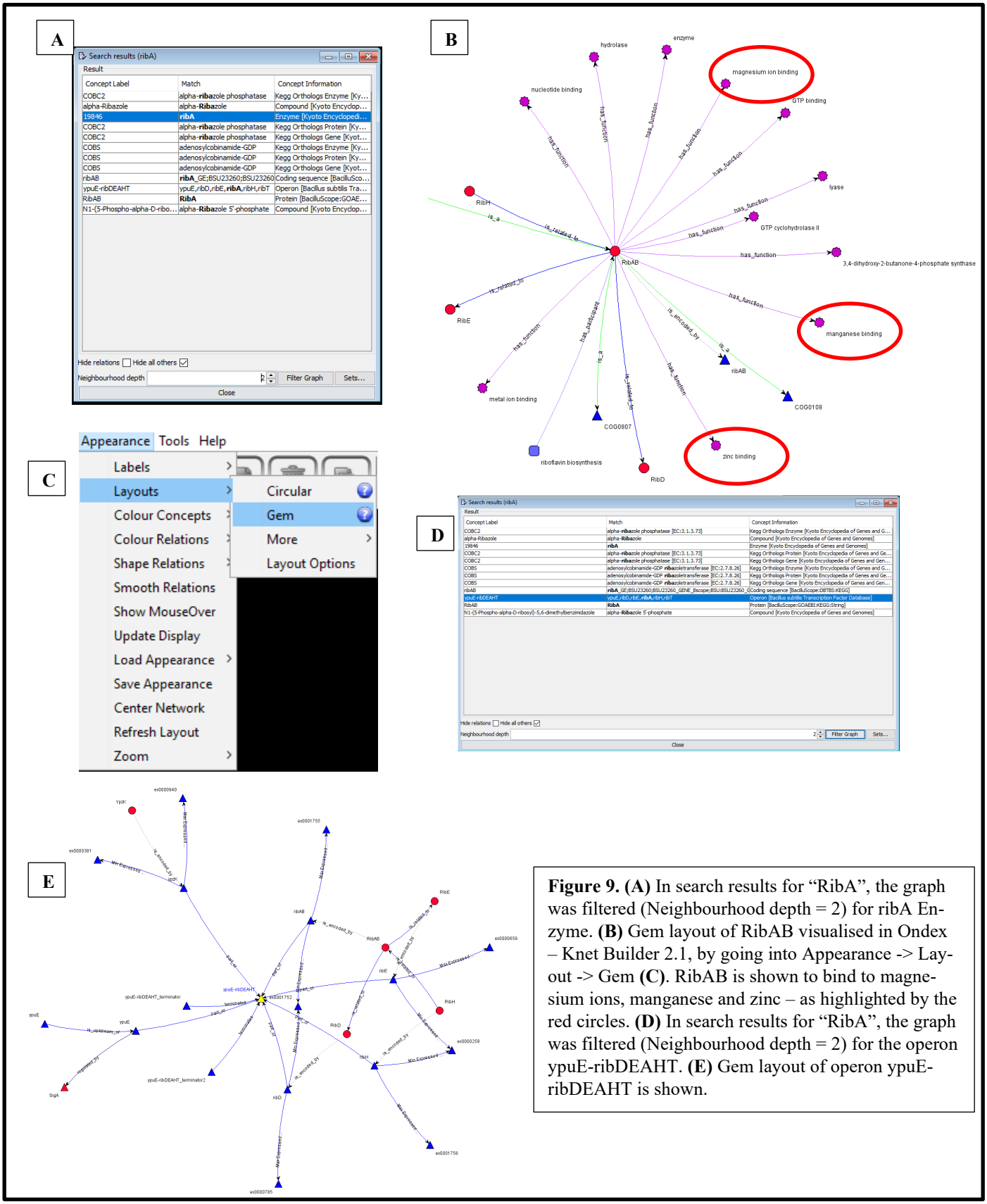

Figure 9. (A) In search results for "RibA", the graph was filtered (Neighbourhood depth = 2) for ribA Enzyme. **(B)** Gem layout of RibAB visualised in Ondex – Knet Builder 2.1, by going into Appearance -> Layout -> Gem **(C)**. RibAB is shown to bind to magnesium ions, manganese and zinc – as highlighted by the red circles. **(D)** In search results for "RibA", the graph was filtered (Neighbourhood depth = 2) for the operon ypuE-ribDEAHT. **(E)** Gem layout of operon ypuE-ribDEAHT is shown.

(A)

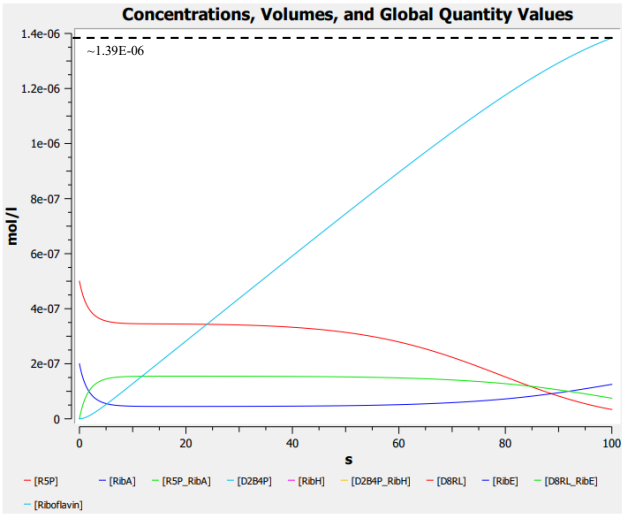

(B)

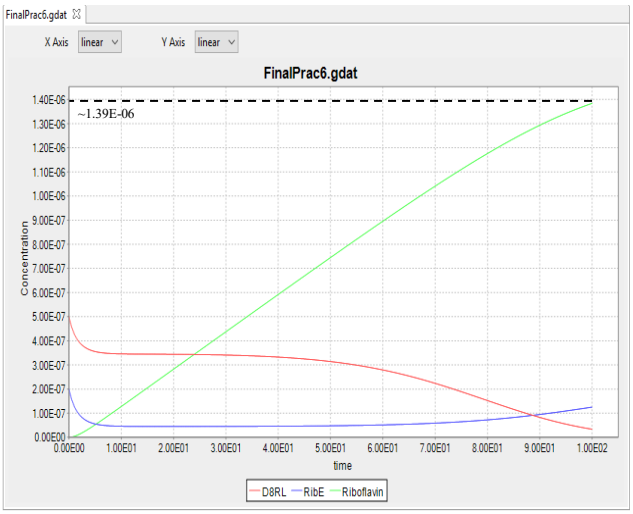

Figure 10. Concentration of Riboflavin over time displayed in **(A)** CopasiUI; **(B)** RuleBender for reactions 1-3 (figure X). In CopasiUI, Riboflavin is represented by the light blue line, D8RL by the red line, RibE by the dark blue line. In RuleBender, D8RL is represented by the red line, RibE by the blue line and riboflavin is represented by the green line. Visually, Riboflavin production is shown to increase at a steady rate, where Vmax has not yet been achieved. [Riboflavin] is shown to be ~ 1.39E-06 mol/l at 100 seconds.

(A)

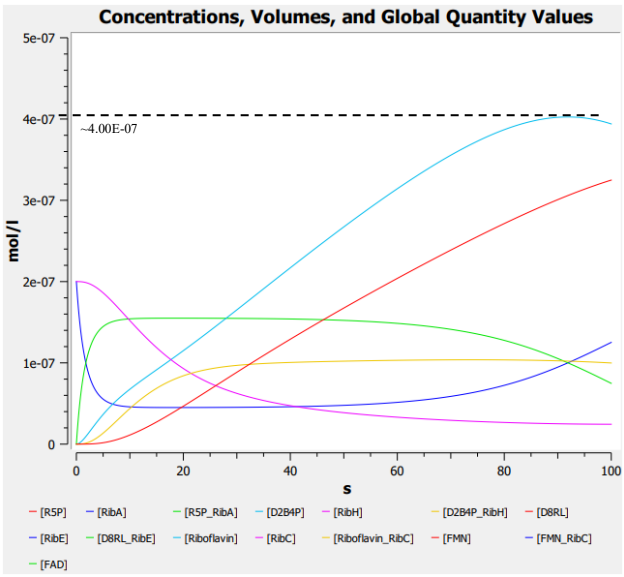

(B)

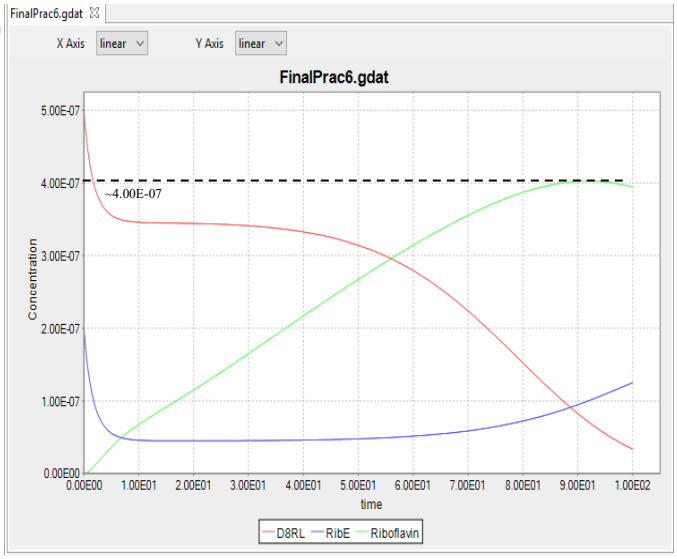

Figure 11. Concentration of Riboflavin over time displayed in **(A)** CopasiUI; **(B)** RuleBender for reactions 1-5 (figure 13). In CopasiUI, Riboflavin is represented by the light blue line, D8RL by the red line, RibE by the dark blue line. In RuleBender, D8RL is represented by the red line, RibE by the blue line and riboflavin is represented by the green line. Visually, Riboflavin production is shown to increase at a steady rate until ~ 9.00E01 seconds, where a plateau is seen at [riboflavin] ~ 4.00E-07 mol/l (Vmax).

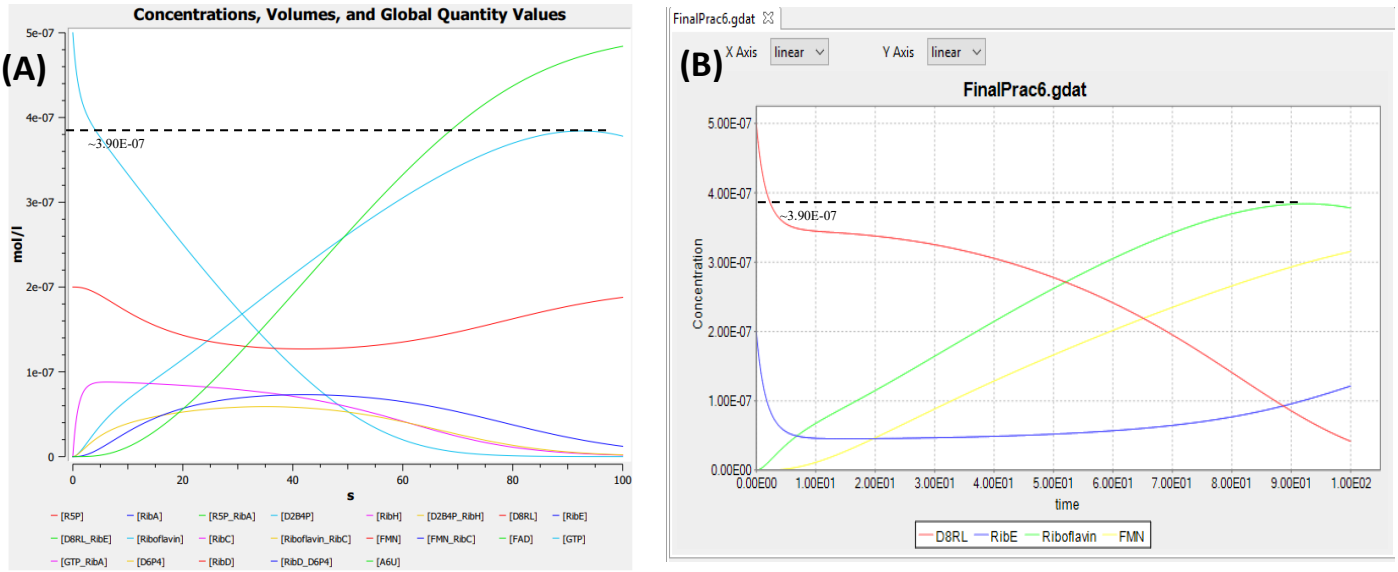

Figure 12. Concentration of Riboflavin over time displayed in **(A)** CopasiUI; **(B)** RuleBender for reactions 1-7 (figure 13). In CopasiUI, Riboflavin is represented by the light blue line, D8RL by the red line, RibE by the dark blue line. In RuleBender, D8RL is represented by the red line, RibE by the blue line, FMN by the yellow line, and riboflavin is represented by the green line. Visually, Riboflavin production is shown to increase at a steady rate, slower than reactions 1-5, until ~ 9.00E01 seconds, where a plateau is seen at [riboflavin] ~3.90E-07 mol/l (Vmax).

Reactions:

```
1  R5P  + RibA  -> R5P_RibA;      (k1 * RibA * R5P);
   R5P_RibA     -> R5P + RibA;    (k1r * R5P_RibA );
   R5P_RibA     -> RibA + D2B4P;  (k2 * R5P_RibA);

2  D2B4P +RibH  -> D2B4P_RibH;    (k1 * RibH * D2B4P);
   D2B4P_RibH   -> RibH + D2B4P;  (k1r * D2B4P_RibH);
   D2B4P_RibH   -> RibH + D8RL;   (k2 * D2B4P_RibH);

3  D8RL+RibE    -> D8RL_RibE;    (k1 * RibE * D8RL);
   D8RL_RibE    -> RibE + D8RL;  (k1r * D8RL_RibE);
   D8RL_RibE    -> RibE + Riboflavin; (k2 * D8RL_RibE);

4  RibC + Riboflavin -> Riboflavin_RibC;   (k1 * RibC * Riboflavin);
   Riboflavin_RibC   -> RibC + Riboflavin; (k1r * Riboflavin_RibC);
   Riboflavin_RibC   -> RibC + FMN;        (k2 * Riboflavin_RibC);

5  RibC + FMN -> FMN_RibC;                 (k1 * RibC * FMN);
   FMN_RibC   -> RibC + FMN;               (k1r * FMN_RibC);
   FMN_RibC   -> RibC + FAD;               (k2 * FMN_RibC);

6  GTP + RibA   -> GTP_RibA;      (k1 * RibA * GTP);
   GTP_RibA     -> GTP + RibA;    (k1r * GTP_RibA);
   GTP_RibA     -> RibA + D6P4;   (k2 * GTP_RibA);

7  D6P4 + RibD  -> RibD_D6P4;     (k1 * RibD * D6P4);
   RibD_D6P4    -> D6P4 + RibD;   (k1r * RibD_D6P4);
   RibD_D6P4    -> RibD + A6U;   (k2 * RibD_D6P4);
```

Figure 13. Reactions involved in the biosynthesis of riboflavin in *B. Subtilis* (1-7) are displayed in Tellurium

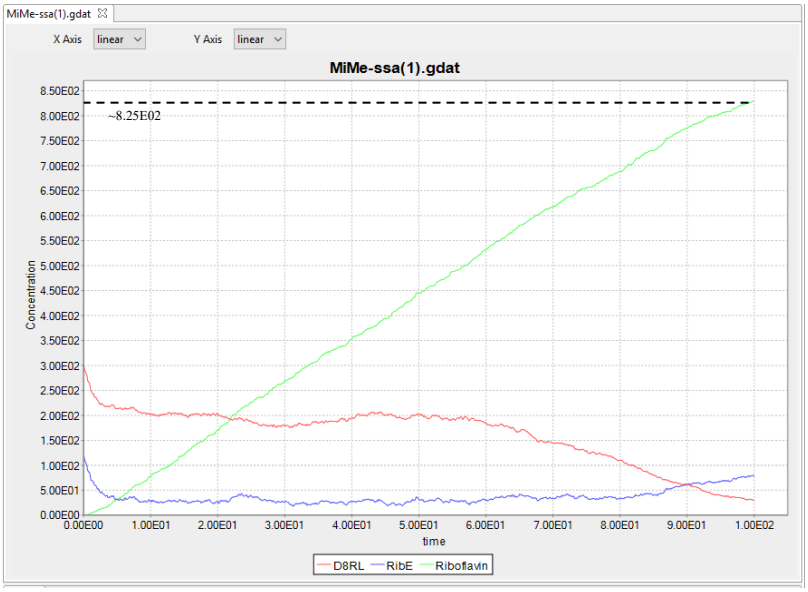

Figure 14. Stochastic simulation of the concentration of riboflavin over time displayed in RuleBender, for reactions 1-3 (figure 13). D8RL is represented by the red line, RibE by the blue line and riboflavin is represented by the green line. Visually, Riboflavin production is shown to increase at a steady rate, where Vmax has not yet been achieved. [Riboflavin] is shown to be ~ 8.25E02 mol/l at 100 seconds.

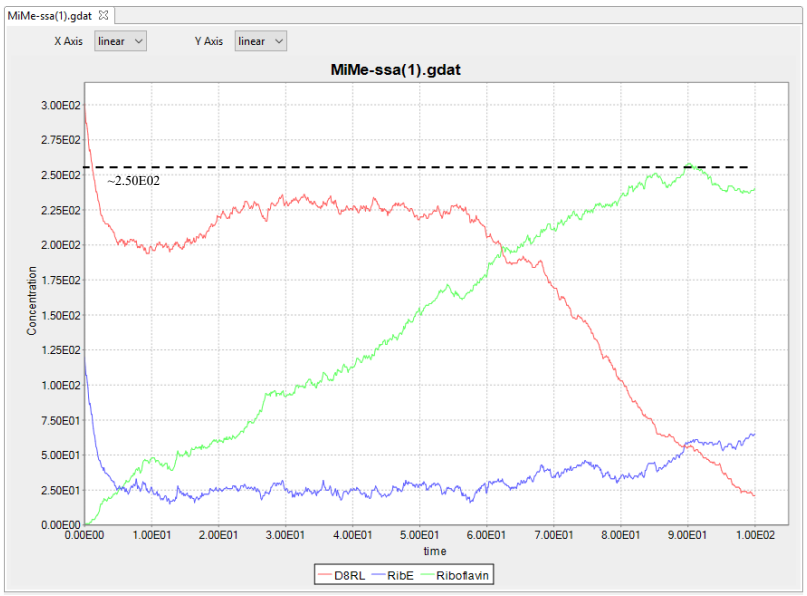

Figure 15. Stochastic simulation of the concentration of riboflavin over time displayed in RuleBender, for reactions 1-5 (figure 13). D8RL is represented by the red line, RibE by the blue line and riboflavin is represented by the green line. Visually, Riboflavin production is shown to increase at a steady rate until Vmax is achieved at ~90 seconds at [riboflavin] ~2.50E02 mol/l

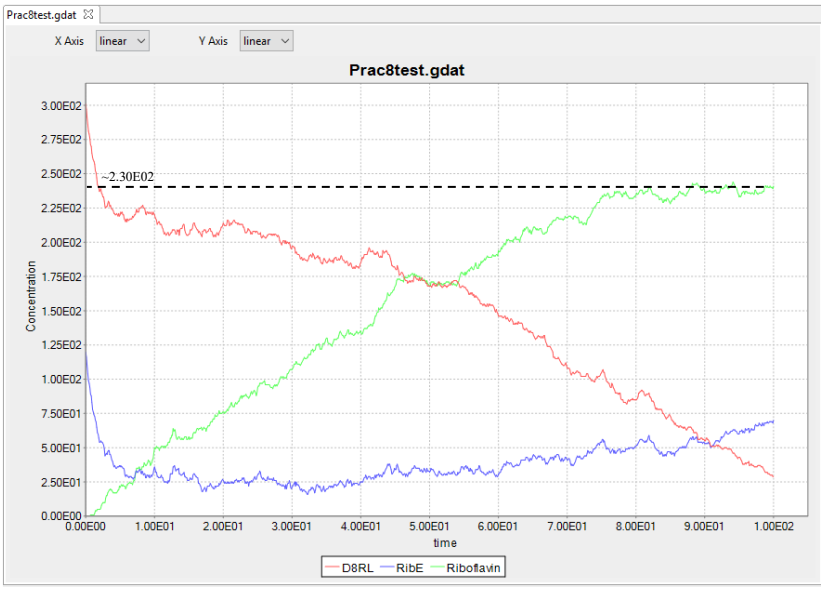

Figure 16. Stochastic simulation of the concentration of riboflavin over time displayed in RuleBender, for reactions 1-7 (figure 13). D8RL is represented by the red line, RibE by the blue line and riboflavin is represented by the green line. Visually, Riboflavin production is shown to increase at a steady rate until Vmax is achieved at ~80 seconds where [riboflavin] is shown to be ~2.30E02 mol/l.

```
begin parameters
    c1      0.00166053904
    c1r     1e-4
    c2      0.1
end parameters

#begin seed species
#   S(a)        5e-7
#   E(a)        2e-7
#   P()     0
#end seed species

begin seed species
    R5P(a)          301
    RibA(a)         120
    D2B4P(a)        301
    RibH(a)         120
    D8RL(a)         301
    RibE(a)         120
    Riboflavin(a)   0
    RibC(a)         120
    FMN(a)          0
    FAD()          0
    GTP(a)          301
    D6P4(a)         0
    RibD(a)         120
    A6U()          0

end seed species


begin reaction rules
    R5P(a) + RibA(a) <-> R5P(a!1).RibA(a!1) c1, c1r
    R5P(a!1).RibA(a!1) -> D2B4P(a) + RibA(a) c2

    D2B4P(a) + RibH(a) <-> D2B4P(a!1).RibH(a!1) c1, c1r
    D2B4P(a!1).RibH(a!1) -> D8RL(a) + RibH(a) c2

    D8RL(a) + RibE(a) <-> D8RL(a!1).RibE(a!1) c1, c1r
    D8RL(a!1).RibE(a!1) -> Riboflavin(a) + RibE(a) c2

    Riboflavin(a) + RibC(a) <-> Riboflavin(a!1).RibC(a!1) c1, c1r
    Riboflavin(a!1).RibC(a!1) -> FMN(a) + RibC(a) c2

    FMN(a) + RibC(a) <-> FMN(a!1).RibC(a!1) c1, c1r
    FMN(a!1).RibC(a!1) -> FAD() + RibC(a) c2

    GTP(a) + RibA(a) <-> GTP(a!1).RibA(a!1) c1, c1r
    GTP(a!1).RibA(a!1) -> D6P4(a) + RibA(a) c2

    D6P4(a) + RibD(a) <-> D6P4(a!1).RibD(a!1) c1, c1r
    D6P4(a!1).RibD(a!1) -> A6U() + RibD(a) c2

end reaction rules
```

```
begin observables
    Molecules   RibA        RibA(a)
    Molecules   R5P         R5P(a)
    Molecules   D2B4P       D2B4P(a)

    Molecules   RibH        RibH(a)
    Molecules   D8RL        D8RL(a)

    Molecules   RibE        RibE(a)
    Molecules   Riboflavin  Riboflavin(a)

    Molecules   RibC        RibC(a)
    Molecules   FMN         FMN(a)

    Molecules   FAD         FAD()

    Molecules   GTP         GTP(a)
    Molecules   D6P4        D6P4(a)

    Molecules   RibD        RibD(a)
    Molecules   A6U         A6U()
end observables

## actions ##
generate_network({overwrite=>1})

# Equilibration
simulate_ssa({t_end=>100,n_steps=>1000})
```

Figure 17. RuleBender code for generating SSA (Stochastic Simulation Algorithm). Calculations for stochastic rate parameters shown in Table X.

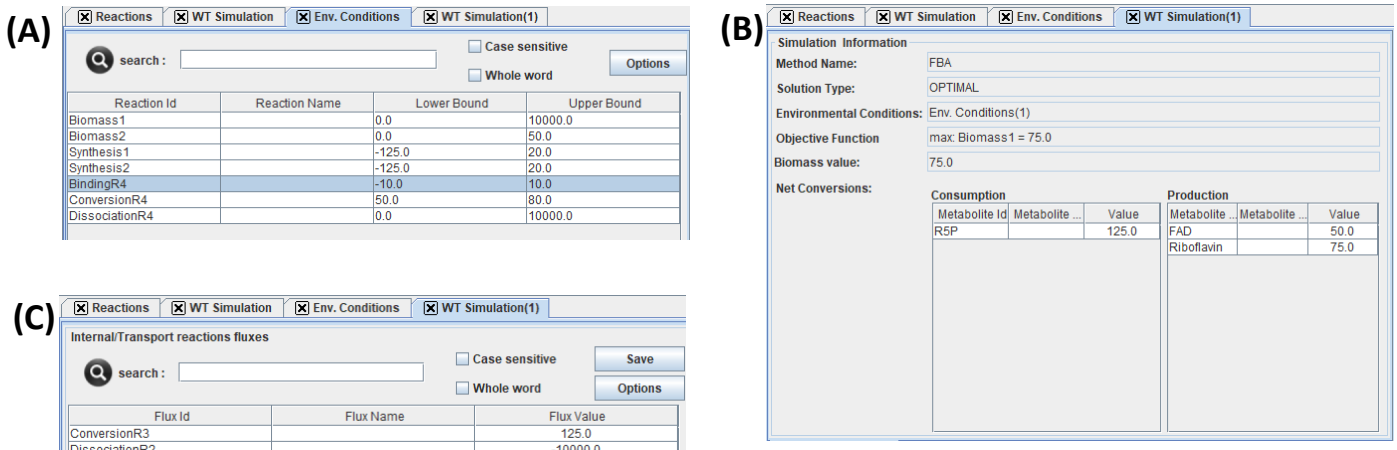

Figure 18. Flux Balance Analysis on the Michaelis-Menten enzymic reactions 1-7 shown in figure 13. **(A)** Environmental conditions, where lower and upper bounds are displayed, **(B)** Net conversions of **1)** consumption of R5P shown to be 125, **2)** Production of FAD: 50; Riboflavin: 75. **(C)** Internal/Transport reaction values are shown.

```
// Reactions:

Synthesis1: -> R5P;    (k_R5P);
Synthesis2: -> GTP;    (k_GTP);
Biomass1:  Riboflavin ->;   (k_Riboflavin * Riboflavin);
Biomass2:  FAD ->;   (k_FAD * FAD);

BindingR1: R5P  + RibA  -> R5P_RibA;      (k1 * RibA * R5P);
DissociationR1: R5P_RibA     -> R5P + RibA;    (k1r * R5P_RibA );
ConversionR1: R5P_RibA     -> RibA + D2B4P;  (k2 * R5P_RibA);

BindingR2: D2B4P +RibH  -> D2B4P_RibH;    (k1 * RibH * D2B4P);
DissociationR2: D2B4P_RibH   -> RibH + D2B4P;  (k1r * D2B4P_RibH);
ConversionR2: D2B4P_RibH   -> RibH + D8RL;   (k2 * D2B4P_RibH);

BindingR3: D8RL+RibE    -> D8RL_RibE;    (k1 * RibE * D8RL);
DissociationR3: D8RL_RibE    -> RibE + D8RL;  (k1r * D8RL_RibE);
ConversionR3: D8RL_RibE    -> RibE + Riboflavin; (k2 * D8RL_RibE);

BindingR4: RibC + Riboflavin -> Riboflavin_RibC;   (k1 * RibC * Riboflavin);
DissociationR4: Riboflavin_RibC   -> RibC + Riboflavin; (k1r * Riboflavin_RibC);
ConversionR4:  Riboflavin_RibC   -> RibC + FMN;        (k2 * Riboflavin_RibC);

BindingR5: RibC + FMN -> FMN_RibC;                (k1 * RibC * FMN);
DissociationR5: FMN_RibC   -> RibC + FMN;              (k1r * FMN_RibC);
ConversionR5: FMN_RibC   -> RibC + FAD;              (k2 * FMN_RibC);

BindingR6: GTP + RibA   -> GTP_RibA;      (k1 * RibA * GTP);
DissociationR6: GTP_RibA     -> GTP + RibA;    (k1r * GTP_RibA);
ConversionR6: GTP_RibA     -> RibA + D6P4;   (k2 * GTP_RibA);

BindingR7: D6P4 + RibD  -> RibD_D6P4;     (k1 * RibD * D6P4);
DissociationR7: RibD_D6P4    -> D6P4 + RibD;   (k1r * RibD_D6P4);
ConversionR7: RibD_D6P4    -> RibD + A6U;   (k2 * RibD_D6P4);
```

Figure 19. Tellurium code for Flux Balance Analysis in OptFlux. Two synthesis reactions were created for R5P and GTP, and two biomass reactions created for Riboflavin and FAD.

References

1. Sonenshein AL, et al. Bacillus subtilis and its closest relatives: From genes to cells. ASM Press; 2002.
2. Vincent Sewalt, Diane Shanahan, Lori Gregg, James La Marta, and Roberto Carrillo. Industrial Biotechnology. Oct 2016.
3. Kabisch J, Thürmer A, Hübel T, Popper L, Daniel R, Schweder T. Characterization and optimization of Bacillus subtilis ATCC 6051 as an expression host. J Biotechnol 2013;163(2):97–104
4. National Center for Biotechnology Information. PubChem Database. Riboflavin, CID=493570
5. Lykstad J, Sharma S. StatPearls [Internet]. StatPearls Publishing; Treasure Island (FL): Feb 16, 2019. Biochemistry, Water Soluble Vitamins.
6. Balasubramaniam S, Christodoulou J, Rahman S. Disorders of riboflavin metabolism. J. Inherit. Metab. Dis. 2019 Jul;42(4):608-619.
7. Finsterer J. An update on diagnosis and therapy of metabolic myopathies. Expert Rev Neurother. 2018 Dec;18(12):933-943.
8. Peechakara BV, Gupta M. StatPearls [Internet]. StatPearls Publishing; Treasure Island (FL): May 15, 2019. Vitamin B2 (Riboflavin)
9. Stahmann KP, Revuelta JL, Seulberger H. Three biotechnical processes using Ashbya gossypii, Candida famata, or Bacillus subtilis compete with chemical riboflavin production. Appl Microbiol Biotechnol. 2000;53(5):509–16.]
10. Kupfer E. 1995. Purification of riboflavin. Patent application EP 0 730 034, F Hoffmann-La Roche AG.
11. Bretzel W, Schurter W, Ludwig B, Kupfer E, Doswald S, Pfister M, et al. Commercial riboflavin production by recombinant Bacillus subtilis: down-stream processing and comparison of the composition of riboflavin produced by fermentation or chemical synthesis. Journal of Industrial Microbiology and Biotechnology [Internet]. Springer Nature; 1999 Jan 1;22(1):19–26. Available from: http://dx.doi.org/10.1038/sj.jim.2900604
12. Coquard D, M Huecas, M Ott, JM van Dijl, APGM van Loon and HP Hohmann. 1997. Molecular cloning of the ribC gene from Bacillus subtilis: a point mutation in ribC results in riboflavin overproduction. Mol Gen Genet 254: 81–84.
13. Mack M, APGM van Loon and H-P Hohmann. 1998. Regulation of riboflavin biosynthesis in Bacillus subtilis is affected by the activity of the flavokinase/FAD-synthetase encoded by ribC. J Bacteriol 180: 950–955.
14. Ludwig, H. C., Lottspeich, F., Henschen, A., Ladenstein, R., and Bather, A. (1987) J. Biol. Chem. 262, 1016-1021
15. Ladenstein, R., Schneider, M., Huber, R., Bartunik, H.-D., Wilson. K. Schott. K. and Bather. A. (1988) J. Mol. Biol. 203, 1045-1070
16. F. Kunst , N. Ogasawara , I. Moszer , A. M. Albertini , G. Alloni , V. Azevedo , M. G. Bertero , P. Bessieres , A. Bolotin , S. Borchert , R. Borriss , L. Boursier , A. Brans , M. Braun , S. C. Brignell , S. Bron , S. Brouillet , C. V. Bruschi , B. Caldwell , V. Capuano , N. M. Carter , S. K. Choi , J. J. Codani , I. F. Connerton and A. Danchin , et al., Nature, 1997, 390 , 249 —256
17. hi , Z. Zhang , X. Chen , T. Chen and X. Zhao , Biochem. Eng. J., 2009, 46 , 28 —33
18. I. Thiele and B. O. Palsson , Nat. Protocols, 2010, 5 , 93 —121
19. M. Durot , P. Y. Bourguignon and V. Schachter , FEMS Microbiol. Rev., 2009, 33 , 164 —190
20. H. U. Kim , S. B. Sohn and S. Y. Lee , Biotechnol. J., 2012, 7 , 330 —342
21. S. Shi , T. Chen , Z. Zhang , X. Chen and X. Zhao , Metab. Eng., 2009, 11 , 243 —252
22. Draw.io flowchart software - https://www.draw.io/
23. KEGG pathway - Kanehisa, M. and Goto, S.; KEGG: Kyoto Encyclopedia of Genes and Genomes. Nucleic Acids Res. 28, 27-30 (2000).
24. Szklarczyk D, Gable AL, Lyon D, Junge A, Wyder S, Huerta-Cepas J, Simonovic M, Doncheva NT, Morris JH, Bork P, Jensen LJ, von Mering C.STRING v11: protein-protein association networks with increased coverage, supporting functional discovery in genome-wide experimental datasets. Nucleic Acids Res. 2019 Jan; 47:D607-613.
25. Shannon P, Markiel A, Ozier O, Baliga NS, Wang JT, Ramage D, Amin N, Schwikowski B, Ideker T. Cytoscape: a software environment for integrated models of biomolecular interaction networks. Genome Research 2003 Nov; 13(11):2498-504
26. Ondex -Knet Builder 2.1 software - https://github.com/Rothamsted/ondex-knet-builder
27. G. Misirli, A. Wipat, J. Mullen, K. James, M. Pocock, W. Smith, N. Allenby, J. Hallinan. BacillOndex: An Integrated Data Resource for Systems and Synthetic Biology in Journal of Integrative Bioinformatics, 10(2):224, 2013.
28. Chen L, Wang RS, Zhang XS (2009) Biomolecular networks: methods and applications in systems biology. Wiley, Hoboken
29. de Jong H (2002) Modelling and simulation of genetic regulatory systems: a literature review. J Comput Biol 9(1):67–103
30. Le Novère N, Endler L. Using chemical kinetics to model biochemical pathways. Methods Mol Biol. 2013;1021:147–167.
31. Vannitsem S. Stochastic modelling and predictability: analysis of a low-order coupled ocean-atmosphere model. Philos Trans A Math Phys Eng Sci. 2014;372(2018):20130282.
32. Ledesma-Amaro, Rodrigo et al. “Metabolic engineering of riboflavin production in Ashbya gossypii through pathway optimization.” Microbial cell factories vol. 14 163. 14 Oct. 2015, doi:10.1186/s12934-015-0354-x
33. Aronson, Jeffrey K, and Robin E Ferner. “The law of mass action and the pharmacological concentration-effect curve: resolving the paradox of apparently non-dose-related adverse drug reactions.” British journal of

clinical pharmacology vol. 81,1 (2016): 56-61. doi:10.1111/bcp.12706
34. Birkenmeier, M., et al. (2014). "Kinetic modeling of riboflavin biosynthesis in Bacillus subtilis under production conditions." Biotechnology Letters 36(5): 919-928.
35. Covert MW, Palsson BO. Transcriptional regulation in constraints-based metabolic models of Escherichia coli, J Biol Chem , 2002, vol. 277 (pg. 28058-64)
36. Medley JK, Choi K, König M, Smith L, Gu S, Hellerstein J, et al. (2018) Tellurium notebooks—An environment for reproducible dynamical modeling in systems biology. PLoS Comput Biol 14(6): e1006220. doi:10.1371/journal.pcbi.1006220
37. Smith, A.M., Xu, W., Sun, Y. et al. RuleBender: integrated modeling, simulation and visualization for rule-based intracellular biochemistry. BMC Bioinformatics 13, S3 (2012) doi:10.1186/1471-2105-13-S8-S3
38. Rocha, I., Maia, P., Evangelista, P. et al. OptFlux: an open-source software platform for in silico metabolic engineering. BMC Syst Biol 4, 45 (2010) doi:10.1186/1752-0509-4-45